Introduction to Molecular Neuroimaging Applications

6

Elizabeth Tong and Ghiam Yamin

Molecular imaging (MI) allows the visualization, characterization, and quantification of biologic processes at the molecular level. Originating from the field of nuclear medicine, MI has evolved into a multidisciplinary field, merging knowledge from the fields of cell/molecular biology, chemistry, physics, bioinformatics, and pharmacology. Moving beyond anatomic depiction, MI includes a wide array of strategies to produce and capture imaging signals from cellular processes. Propelled by advances in molecular/cell biology knowledge, as well as emergence of novel imaging techniques and probes, its repertoire is rapidly expanding. Applications and areas of active research encompass the fields of microbiology, immunology, molecular biology, pharmacology, and cancer research.

Generally, nuclear medicine utilizes radiolabeled tracers to produce signals from radioactive decay; MI uses those and other probes that incorporate substrates, ligands, antibodies, or reporter genes to specifically interact with cellular or subcellular targets. Besides positron emission tomography (PET) and single-photon emission computed tomography (SPECT), MI can produce images by capturing magnetism (using MRI), sound (using ultrasound), and bioluminescence or fluorescence (using optical techniques).

The ability to visualize cellular and molecular pathways illuminates the mechanism of diseases on the genetic, molecular, and pathophysiological levels. Many MI techniques are successfully translated from ex vivo experiments to in vivo clinical applications. These advances can potentially lead to early detection of disease, confirmation of diagnosis, selecting disease-specific and patient-specific therapies (personalized medicine), delivering targeted therapy, and monitoring treatment response or disease progression. Pharmaceutical companies also leverage MI for drug discovery.

E. Tong (✉) · G. Yamin
Stanford Health Care, Department of Neuroimaging & Neurointervention, Stanford, CA, USA

Molecular Imaging Agents

Molecular imaging agents are designed to selectively highlight their target and therefore are often termed "smart contrast agents." Target selection is a critical challenge, as the pathophysiology of diseases is often complex or even elusive. Ideal targets are accessible, distinctive, specific, and abundant. Proteins are popular targets of MI agents. Proteins are involved in many cellular activities, for instance, as ligands and receptors for signaling and as enzymes or modulators for activation or deactivation. A protein's specialized functionality is dictated by its unique amino acid composition and morphology. Due to readily accessibility, proteins expressed on the cell surface or in the extracellular space are desirable targets [1]. Building materials for cell synthesis, genetic material, and metabolites are also potential MI targets.

Similar to conventional cross-sectional imaging agents (iodinated contrast for CT and gadolinium for MRI), MI agents are mostly delivered in the bloodstream. However, conventional imaging agents are blood-pool agents and the signal enhancement depends on tissue vascularity and leakiness. On the contrary, MI agents exit the bloodstream in search of their designated target. The signal enhancement depends on the selective accumulation at their targets, avoidance of undestined uptake, and generation of detectable signal in the appropriate setting. This is accomplished by the strategically designed MI agents and delivery vehicles.

There are many novel strategies for designing targeted MI agents. The MI agent can be delivered in the "inactive" form, which is subsequently "activated" when it reaches and binds its designated ligand or receptor. Upon activation, detectable signal is generated to form images. Alternately, an active MI agent can be bound to an inhibitor until it reaches the target, whereupon an enzyme residing in the microenvironment cleaves the bond and releases the inhibitor. The freed active MI agent will then bind to the target. Instead of an inhibitor, the active MI agent can be bound with specific antibodies, which seek and bind to the intended ligands (Fig. 6.1) [2].

A. M. Franceschi, D. Franceschi (eds.), *Hybrid PET/MR Neuroimaging*, https://doi.org/10.1007/978-3-030-82367-2_6

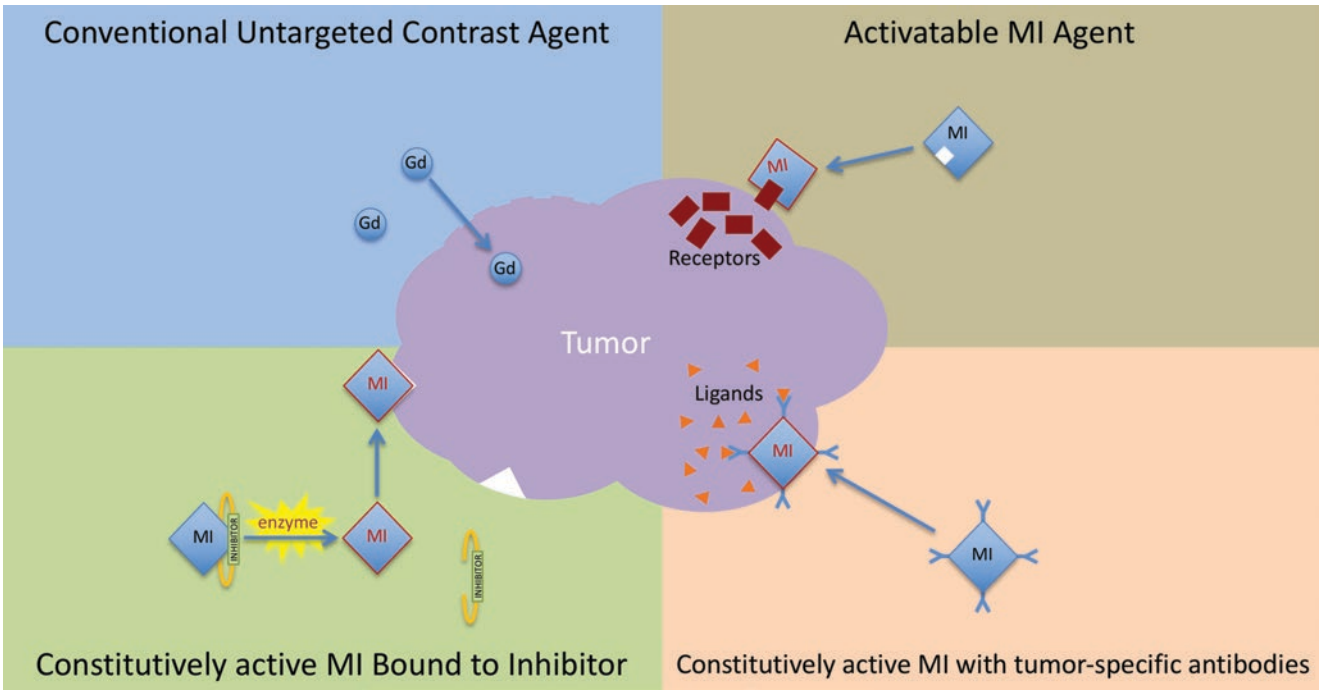

Fig. 6.1 Design of "smart" molecular imaging (MI) agents. *Upper left panel:* Conventional contrast agents like gadolinium (Gd) crosses leaky vasculature. *Lower left panel:* Active MI agents bound to an inhibitor are released when an enzyme (present in the appropriate microenvironment) cleaves the inhibitor. *Upper right panel:* Inactive MI agent becomes activated when it reaches the target and binds with the intended ligand or receptor. *Lower right panel:* Active MI agent affixed with antibodies is delivered to the destined recipient

Once MI agents reach their target, the next challenge is signal amplification suitable for detection. Biochemical interactions can help retain MI agents in target tissues. For instance, by substituting ^{18}F for the normal hydroxyl group at the C-2 position, [^{18}F]fluorodeoxyglucose ([^{18}F]FDG) acts as a glucose analog. Without the 2-hydroxyl, however, [^{18}F]FDG cannot undergo glycolysis, accumulates in cells after phosphorylation, and generates signal through radioactive decay. Thus, [^{18}F]FDG uptake is a good reflection of cellular metabolism. Signal amplification can also occur in specific environments. One example is amplified fluorescent signal from a dye linked to a peptide activated after cleavage by matrix metalloproteinase (MMP) present in metastasizing tumors [3].

Molecular Imaging Applications

Most cells generally perform four main functions—structural support, signaling and transport, metabolism (including synthesis and perfusion), and homeostasis (including defense and repair). Conventional contrast agents and traditional imaging methods highlight static structure at the anatomic, tissue, and cellular levels. Cellular functions can now be visualized with molecular imaging. Many players come together to carry out these functions—including those that serve active and regulatory roles. With advances in molecular imaging and better understanding of the complex pathways, we are now able to see some of the processes related to normal brain function and, more interestingly, in CNS pathologies. All the components involved in these pathways are potential targets for molecular imaging. A seemingly endless number of neuro-specific molecular imaging tracers have and continue to appear with applications to a wide breadth of diseases. The purpose of this introduction is not to review them all, but rather to explore a few examples from each class, based on the mechanism of action.

Signaling and Transport

The brain is an elaborate network of neurons that communicate via neurotransmitters. Neurotransmitters influence and regulate a wide range of processes including mentation, emotions, behavior, and stress response. Generally, synaptic transmission starts with synthesizing and loading neurotransmitters into intracellular vesicles. When triggered, packaged neurotransmitters are released into the synaptic cleft and upon binding to the postsynaptic receptors, signal transduction is activated. The neurotransmitters are then metabolized or recycled. Traditionally, this communication has been analyzed through immunohistochemical labeling of synaptic proteins and electron microscopy. With emerging MI agents targeting the different components involved, synaptic communication can now be visualized in vivo.

Levodopa (L-DOPA), which is converted from L-tyrosine by tyrosine hydroxylase, is a precursor the catecholamines/neurotransmitters dopamine, norepinephrine, and epinephrine (Fig. 6.2a) [4]. [^{18}F]Fluorodopa (i.e., [^{18}F]FDOPA), an analog of L-DOPA, is used in PET to assess the nigrostriatal dopamine system in the evaluation of parkinsonian syn-

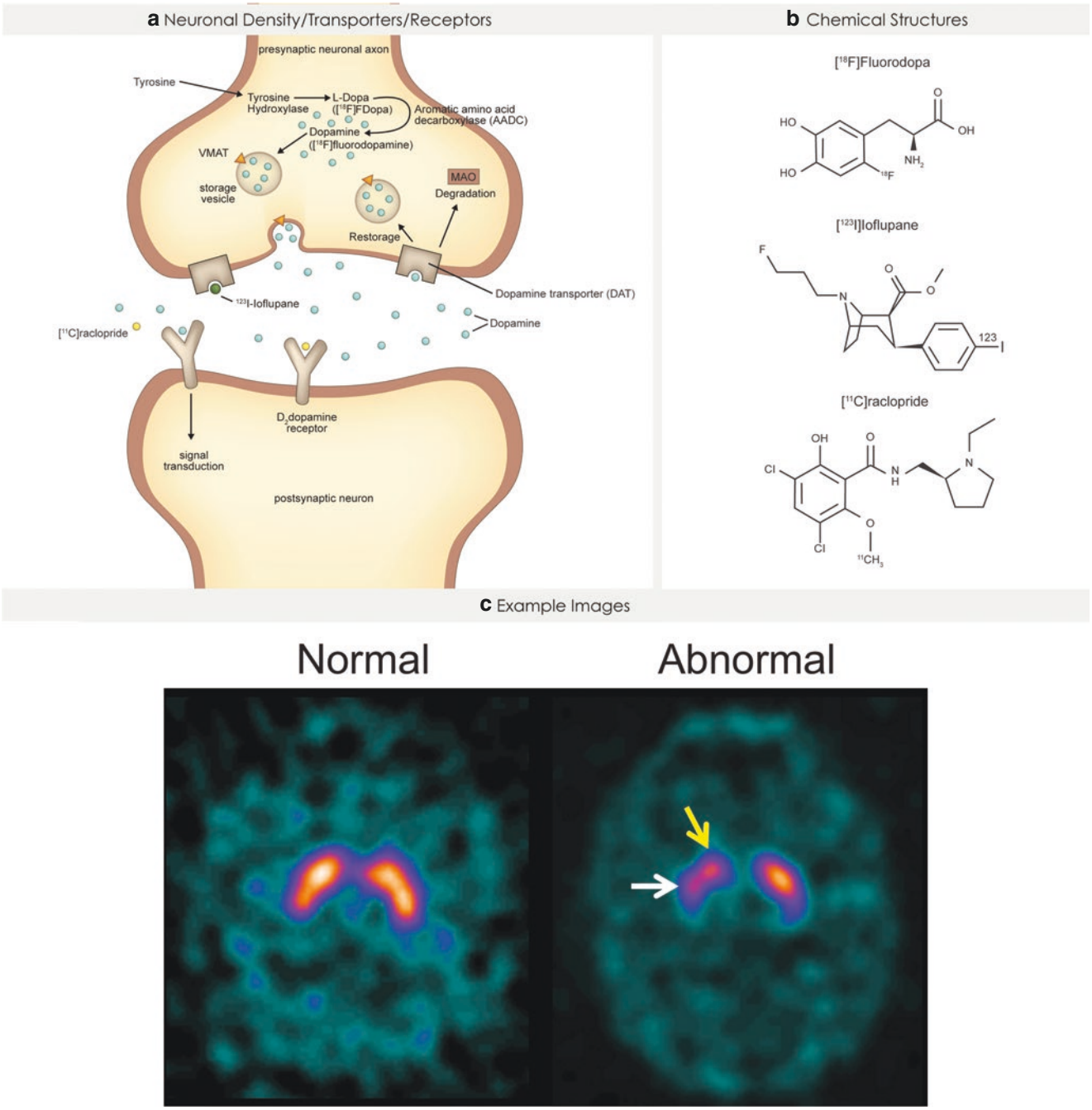

Fig. 6.2 Targets of pre- and postsynaptic dopaminergic targets. (**a**) Dopamine is synthesized in the presynaptic neuron from tyrosine to L-DOPA and converted to dopamine by aromatic amino acid decarboxylase (AADC). Vesicular monoamine transporter 2 (VMAT2) then packages and stores dopamine into vesicles. Upon release, dopamine binds to dopamine receptors expressed on postsynaptic neurons. Dopamine reuptake in presynaptic neurons occurs via the dopamine transporter (DAT). (**b**) Dopamine-related MI agents include (1) [^{18}F] DOPA (FDOPA), an analogue of L-DOPA; (2) [^{123}I]Ioflupane, which binds to the presynaptic dopamine transporter (DAT); and (3) [^{11}C] raclopride, which binds to D_2 dopamine receptors. (**c**) Axial [^{123}I] Ioflupane SPECT images from two different age-matched patients. Left image from a 67-year-old man with a left had tremor, which shows normal [^{123}I]Ioflupane SPECT showing symmetric uptake in the caudate and putamen bilaterally. Right image from a 62-year-old female with possible REM sleep behavior disorder, which shows abnormal [^{123}I]Ioflupane SPECT showing decreased uptake in the right putamen (white arrow) and to a lesser degree the right caudate (yellow arrow). These findings are consistent with parkinsonian syndrome

dromes [5]. [^{18}F]FDOPA is decarboxylated by aromatic amino acid decarboxylase (AADC) in the striatum to [^{18}F] fluorodopamine, a substrate for vesicular monoamine transporter 2 (VAMT2) (Fig. 6.2a, b). VAMT2 loads presynaptic dopamine into vesicles that can be released through exocytosis. [^{18}F]fluorodopamine cycles through exocytosis, reuptake via the dopamine transporter (DAT), and reloading into vesicles. In theory, this is an irreversible process. However, [^{18}F] fluorodopamine can be metabolized by monoamine oxidase (MAO) to yield [^{18}F]6-fluoro-3,4-dihydroxyphenylacetic acid and subsequently metabolized by COMT to produce [^{18}F]6-fluorohomovanillic acid. Both of these subsequently produced metabolites diffuse out the brain. [^{18}F]FDOPA is used primarily to visualize nerve terminals in the striatum. [^{18}F]FDOPA PET scans are interpreted based on the appearance and shape of the striatum (i.e., the putamen and caudate). Normal uptake in the striatum is comma-shaped, symmetrical, and uniform. Reduced size and shape of the putamen or striatum, either uni- or bilaterally, is abnormal. [^{18}F]FDOPA PET shows accuracy in differentiating Parkinson's disease (PD), including all parkinsonian disorders/atypical Parkinsonism conditions such as progressive supranuclear palsy (PSP) and multiple system atrophy (MSA), from non-Parkinson's movement disorders such as essential tremor. In addition to a role in diagnosing PD and parkinsonian disorders, [^{18}F]FDOPA PET accumulates in and allows for precise location of neuroendocrine tumors outside the CNS (e.g., pheochromocytomas and paragangliomas). Further roles of [^{18}F]FDOPA PET include imaging and treatment planning of gliomas and incidental meningioma detection [6, 7].

[^{123}I]Ioflupane, a cocaine analog, is used with DaTscan™ SPECT imaging to assess the dopamine transporter system for diagnosing PD versus similar-presenting non-degenerative tremors [8]. [^{123}I]Ioflupane binds reversibly to dopamine transporter (DAT) located on presynaptic nerve terminals in the striatum and thus reflects the number of dopaminergic neurons in the substantia nigra. DaTscan™ is interpreted based on the appearance and shape of the striatum. In normal patients, the uptake in the striatum is comma-shaped, symmetric, and uniform (Fig. 6.2c). A reduced size or blunted shape of either the putamen or striatum, either uni- or bilaterally, is seen in PD or parkinsonian syndromes. DaTscan™ can aid in the diagnosis of parkinsonian syndromes including idiopathic PD, MSA, and PSP; however, it is unable to discriminate among these diseases.

[^{11}C]raclopride is a synthetic selective antagonist of D_2 dopamine receptors used in PET to measure striatal D_2 dopamine receptor binding characteristics and thus interrogate a wide range of diseases related to dopamine production, including PD, Huntington disease (HD), psychiatric disorders such as schizophrenia, and drug addiction. [^{11}C]raclopride has been used as a tool to investigate striatal dopaminergic function to differentiate MSA from PD [9]. Other neurodegenerative disorders that are diagnosed by [^{11}C]raclopride include HD, which is characterized by neostriatal interneuronal degeneration (postsynaptic to dopaminergic input). [^{11}C]raclopride can detect significant reductions in striatal dopamine D_2 receptor binding in asymptomatic carriers of the HD mutation (expanded CAG repeat length) and has better sensitivity for disease progression compared to glucose metabolism [^{18}F]FDG [10]. In schizophrenic patients, [^{11}C]raclopride has been used to evaluate neocortical receptor occupancy of antipsychotic drugs in disease treatment [11–14]. In drug addiction research, [^{11}C]raclopride is used as an indirect measure of dopamine release [15]. Dopamine release is blunted in drug dependency compared to normal healthy controls after pharmacologic challenge to either the abused drug or a stimulant. Notably, [^{11}C] raclopride also has a role in assessing treatment response of prolactinomas, a specific type of pituitary tumor, to dopamine agonists [16].

Metabolism (Synthesis and Perfusion)

[^{18}F]FDG, a PET glucose analog, is used as the workhorse predominantly in oncologic assessment. [^{18}F]FDG competes with glucose and is taken up by glucose-dependent cells and thereafter phosphorylated by hexokinase to [^{18}F]FDG 6-phosphate, which is metabolically inert and irreversibly trapped (Fig. 6.3a). A trace amount of the intravenously injected [^{18}F]FDG accumulates in metabolically active cells after phosphorylation and thus provides a reliable quantifiable metric for cellular metabolism. [^{18}F]FDG PET provides high sensitivity and specificity in detecting several types of cancers; however, uptake can also be seen in infection, inflammatory conditions, and a number of other non-oncologic diseases. Normal brain relies entirely on glucose metabolism, and its high metabolism for glucose renders [^{18}F]FDG relatively insensitive to tumor detection. Nevertheless, some high-grade tumor can still be detected over background high brain metabolism due to the principle of the Warburg effect (i.e., specialized fermentation used by cancer cells over aerobic respiration used by normal cells). [^{18}F]FDG serves a more prominent role in primary head and neck cancer and pathologic lymph node detection, which are less confounded by background glucose uptake that can hamper conspicuity. [^{18}F]FDG PET also plays in the role in diagnosis of dementia [17], which can show typical areas of hypometabolism in particular brain regions (Fig. 6.3b). For example, patients with Alzheimer's disease (AD) can show marked hypometabolism in the bilateral prefrontal regions, parietal lobes, temporal lobes, and posterior cingulate–precuneus cortical regions. Hypometabolism in the primary visual cortex is very specific and moderately sensitive for

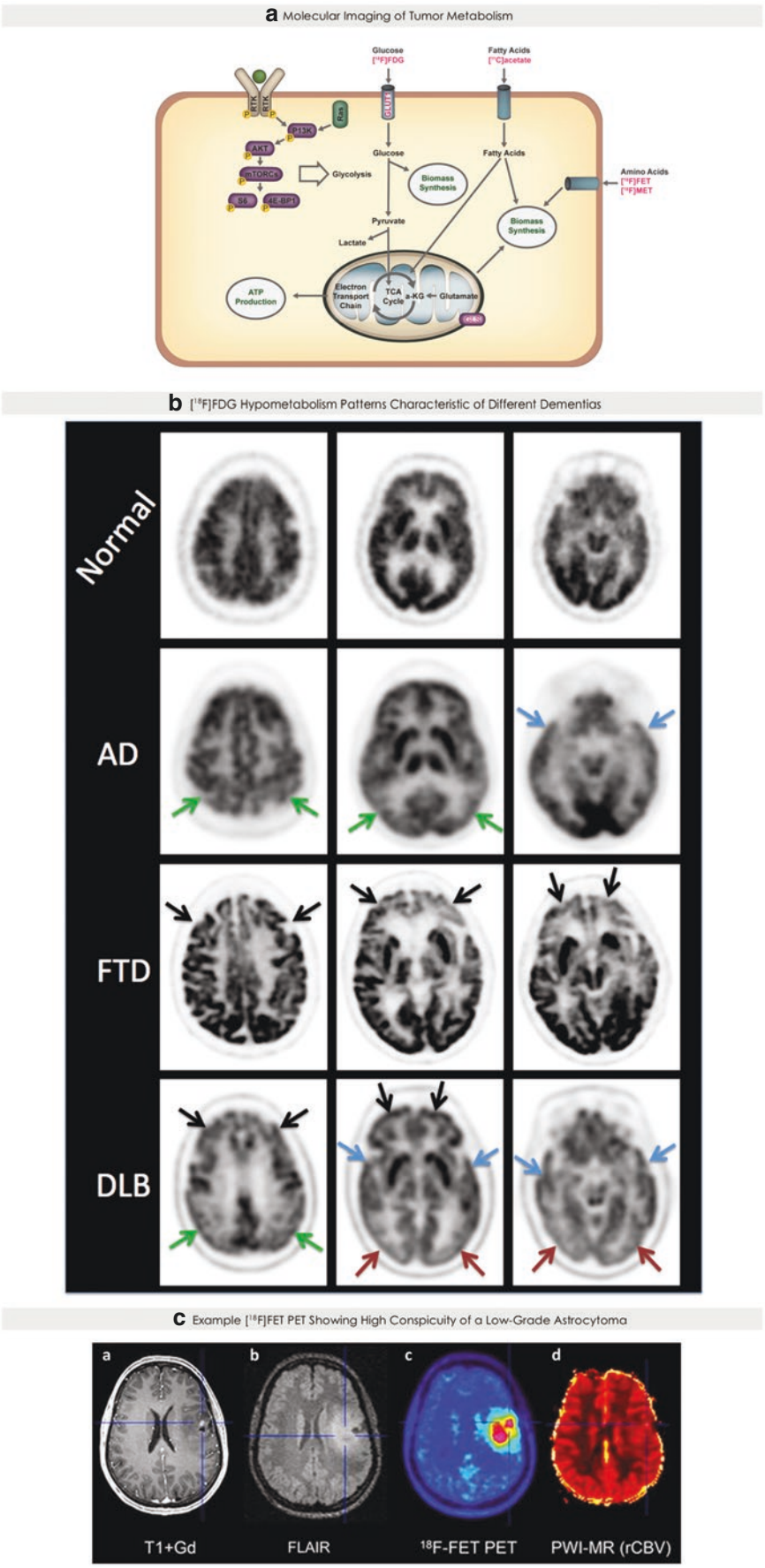

Fig. 6.3 Metabolic pathways that can be visualized by molecular imaging. (**a**) Glucose uptake can be detected by [^{18}F]FDG. Fatty acid uptake can be detected by [^{11}C]acetate. Protein synthesis can be detected with [^{11}C]-methionine (MET) and [^{18}F]-ethyl-tyrosine (FET). (**b**) Axial [^{18}F]FDG PET images from three different dementia patients and one normal control. Top row of images shows PET from a 75-year-old man showing normal FDG metabolism for age. Second row of images shows PET from a 58-year-old woman with a history of memory loss showing moderately decreased FDG metabolism in the bilateral temporoparietal regions (green and blue arrows), consistent with Alzheimer's disease (AD). Third row of images shows PET from a 71-year-old man with a history of cognitive impairment showing FDG hypometabolism in the frontal lobes with overall pattern (black arrows), suggestive of frontal-predominant form of frontotemporal dementia (FTD). Fourth row of images shows PET from a 78-year-old female with a history of visual hallucinations showing global FDG hypometabolism within the frontal (black arrows), temporal (blue arrows), parietal (green arrows), and occipital lobes (red arrows). Most prominent region of hypometabolic activity is within the occipital lobes. Preserved normal FDG activity within the basal ganglia, primary sensorimotor cortices, precuneus, and cerebellum (not shown). These findings favor dementia with Lewy bodies (DLB). (**c**) Hybrid PET/MRI of patient with an astrocytoma (WHO grade II). Contrast-enhanced T1-weighted MR imaging shows a small area of abnormal contrast enhancement (**a**) and corresponding FLAIR hyperintense signal abnormality (**b**) in the left frontal lobe. This is more conspicuous on [^{18}F]FET PET (**c**), which better delineates the large tumor in this region. Tumor is not apparent on the on rCBV map (**d**). (Figure 6.3c reprinted with permission from Filss et al. [39])

distinguishing dementia with Lewy bodies from AD (Fig. 6.3b).

Another method to image metabolism is to capture the biosynthesis of cell constituents (carbohydrates, lipids, proteins, and nucleic acids) by tagging the raw materials (Fig. 6.3). Methionine is an essential amino acid and is the first amino acid integrated into each protein chain, as specified by the genetic code in humans. [^{11}C]-methionine (MET) is an effective MI agent for probing protein synthesis. Compared to normal brain tissue, CNS tumors synthesize more protein to support rapid growth. MET PET is useful in evaluating grade, type, and proliferative activity of primary gliomas (Fig. 6.3c) [18]. Combined with radiomics, MET PET performed well in differentiating radiation necrosis from recurrent brain tumor [19]. The short half-life of ^{11}C (20 min) necessitates an onsite cyclotron and thus limits its clinical utility. The longer half-life (110 min) of [^{18}F]-ethyl-tyrosine (FET) makes it an attractive contender among amino acid-based tracers. FET PET can provide prognostic information on patients with low-grade gliomas and risk stratify cases with disease progression for earlier and more aggressive therapy [20].

Perfusion

Cerebral blood flow can be measured using [^{15}O]H_2O positron emission tomography imaging. [^{15}O]H_2O acts as a freely diffusible tracer that participates in the exchange between blood and cerebral tissue. Immediately after administration, PET counts are collected over a time interval. Studies show that tissue radioactivity and regional cerebral blow flow [rCBF] are almost linearly related across the flow range in humans. Relative rCBF can be measured through integration of PET counts after arrival of the tracer bolus. Absolute rCBF requires kinetic modeling performed with the arterial input function and an one-compartment model [21]. [^{15}O]H_2O PET can accurately reflect the perfusion status in normal brain and in conditions altering regional flow. In vivo brain CBF measurement has been beneficial in the evaluation of cerebrovascular disease and neurodegenerative disorders [22].

An interesting adaptation of the technique is to assess cerebrovascular reactivity (CVR) (Fig. 6.4). CVR is the perfusion response of the cerebral vasculature to stress that results in increased CBF. [^{15}O]H_2O PET is currently regarded as the gold standard for measuring CVR—either inducing hypercapnia via a non-rebreather mask set up for carbon dioxide delivery or by intravascular administration of acetazolamide. Alterations in CBF from baseline are used to estimate CVR. CVR can provide useful information about cerebrovascular condition and regional metabolism. Impaired CVR is an independent predictor of increased risk for ischemic events in patients with carotid stenosis or occlusion [23].

Homeostasis (Defense and Repair)

Increasingly, neuroinflammation is postulated to play a role in neurodegenerative diseases and neuroimmunological disorders; however, its exact role is yet to be fully elucidated. Chronic neuroinflammation, elevated cytokines levels, and activated immune cells are observed in these diseases [24, 25]. Microglia are resident immunocytes and the first line of defense in the brain that maintain homeostasis and protect against infection and damage. Normally quiescent, these cells are activated when exposed to pathogens or neuronal damage and become phagocytic. In response to pathogens, inflammasomes are assembled in microglia. Phagocytosis of amyloid plaques (Aβ) in Alzheimer's disease or fibrillar α-synuclein (α-Syn) in Parkinson's disease activates inflammasomes (Fig. 6.5). Defense or repair is launched through a cascade of inflammatory cytokines. The released interleukins (IL-1β and IL-18) recruit peripheral leukocytes, which then infiltrate the otherwise privileged CNS [26]. Inflammasomes are mainly involved in innate immune response, but also contribute to neuroinflammatory damage (Fig. 6.5) [27].

Many radiotracers and MI agents have been developed for candidate biomarkers of neuroinflammation. As inflammation disrupts the blood-brain barrier (BBB), radioisotopes that monitor vascular permeability (such as $^{99m}TcO_4$, ^{99m}Tc-DTPA, ^{68}Ga-EDTA) have been used to indirectly image neuroinflammation. Radioisotope-labeled leukocytes have also been used in nuclear imaging, but the preparation is laborious—requiring the extraction of white blood cells from the patient and reinjecting into the patient after in vitro tagging with ^{111}In or ^{99m}Tc. Visualizing arachidonic acid, the precursor for key inflammatory mediators (e.g., prostaglandins, thromboxanes, and leukotrienes), has also been investigated (Fig. 6.6) [28].

Newer MI agents target more specific biomarkers of neuroinflammation. The prototypical agent for neuroinflammation imaging is PK11195, which is a ^{11}C-labeled analog of benzodiazepine that binds translocator protein 18 kDa (TSPO). TSPO, a mitochondrial protein upregulated in activated microglia, reactive astrocytes, and macrophages, is an effective target for probing the dynamics of immune activation. PK11195 PET has revealed the role of neuroinflammation in Alzheimer-type dementia [29], in addition to other neurodegenerative diseases such as amyotrophic lateral sclerosis [30] and MSA [31]. Alternate biomarkers, which are upregulated or activated, are being

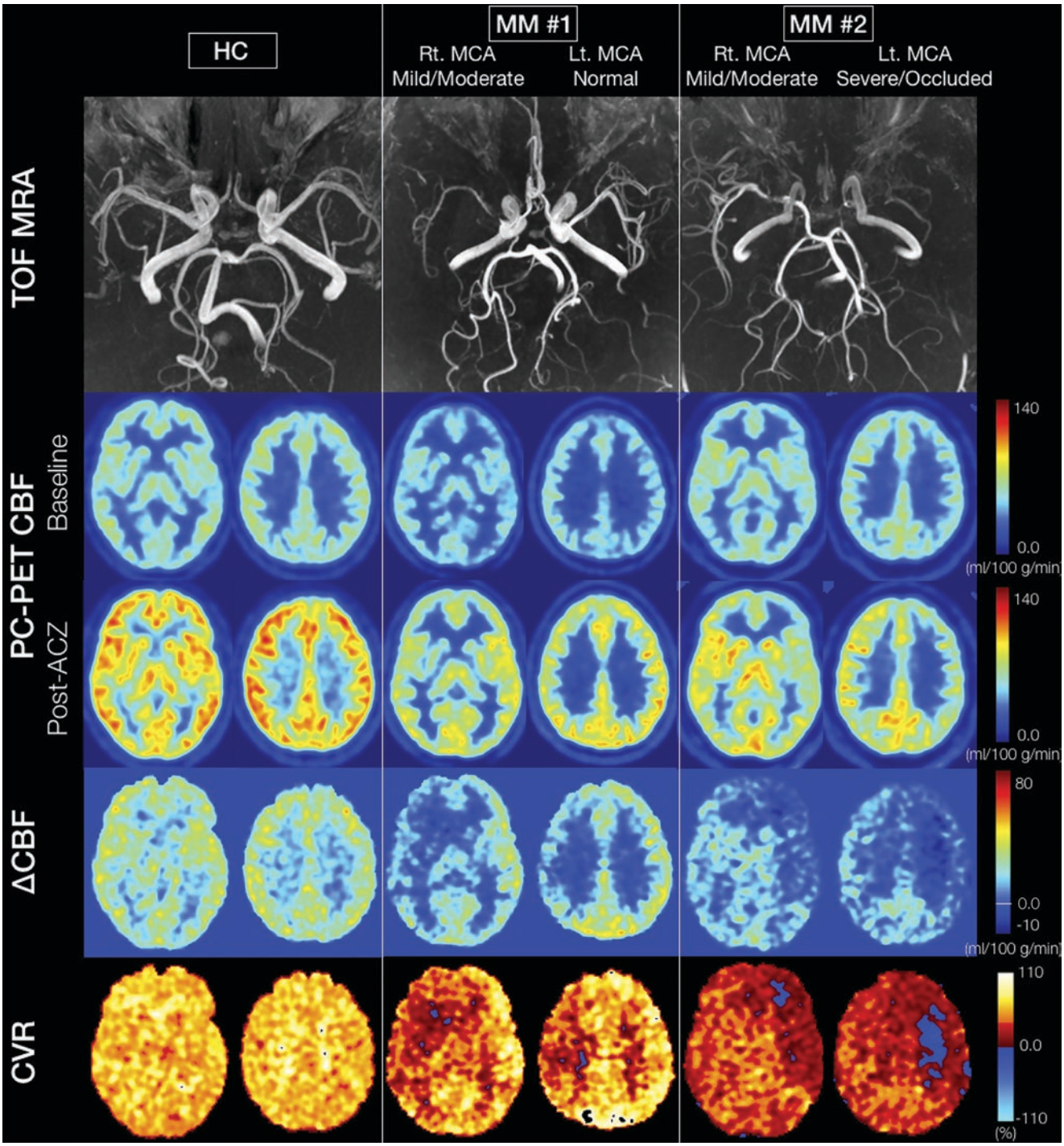

Fig. 6.4 Assessing cerebrovascular reactivity with [^{15}O]H_2O PET. Representative cases: (From the top row) time-of-flight (TOF) MR angiogram, two slices of phase contrast (PC)-PET cerebral blood flow (CBF) at baseline and after acetazolamide (ACZ) administration, change in CBF (ΔCBF), and cerebrovascular reactivity (CVR, %) maps. The left column shows a health control (HC) case. A significant CBF increase is visible in all territories after ACZ. The ΔCBF in the gray matter is larger than in deep white matter, while CVR is essentially constant in all regions for the HC. The middle and right columns show the patients with Moyamoya disease (MM #1 and #2). Both cases present asymmetric stenosis grades of the middle cerebral arteries (MCAs), with normal grades for the bilateral posterior cerebral arteries (PCAs). Bilateral anterior cerebral arteries (ACAs) are graded as normal in Patient #1 and as severe in Patient #2. The post-ACZ is asymmetric, with less CBF increase in the hemisphere with more severe stenosis in both MM cases. Notably, in the left hemisphere of Patient #2, there are regions where the CVR is negative (blue area). Abbreviations: HC healthy control, TOF time of flight, ACZ acetazolamide, PC phase contrast, PET positron emission tomography, CBF cerebral blood flow, CVR cerebrovascular reactivity, MCA middle cerebral artery, PCA posterior cerebral artery, ACA anterior cerebral artery. (Figure reprinted with permission from Ishii et al. [40])

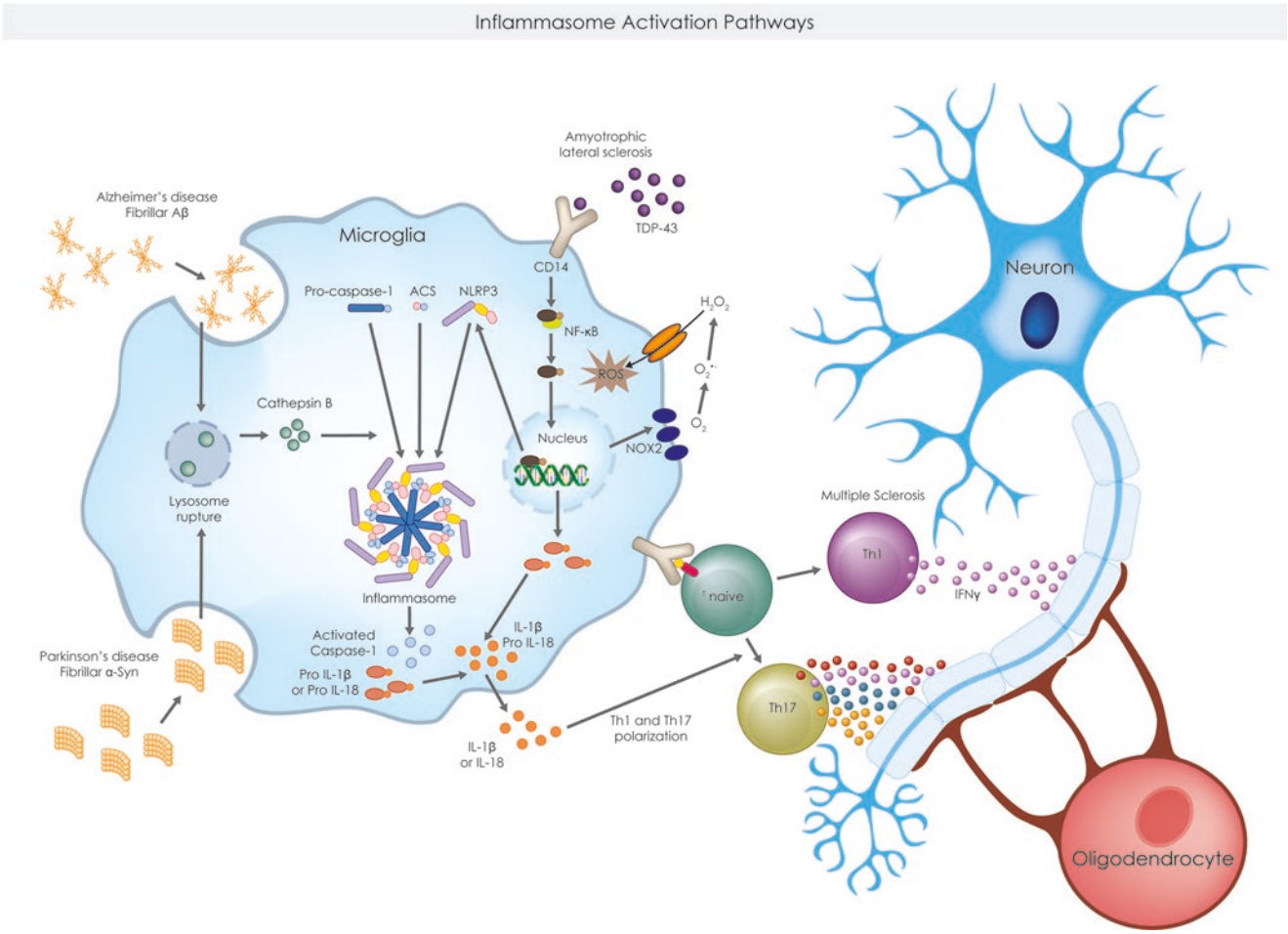

Fig. 6.5 Inflammasome activation pathways in neurodegenerative and neuroimmunological disorders. Inflammasome assembly in CNS inflammatory cells can be triggered by phagocytosis of fibrillar amyloid β (Aβ) in Alzheimer's disease or fibrillar α-synuclein (α-Syn) in Parkinson's disease. Lysosomal rupture after phagocytosis releases cathepsin B, which activates the NLRP3 (NOD-, LRR-, and pyrin domain-containing protein 3) inflammasome. Inflammasomes trigger the release of interleukins (e.g., IL-1β), which promote polarization of helper T-cells (Th). Myelin-specific autoreactive T-cells (Th1 and Th17) cause an inflammatory response, demyelination, and axonal damage seen in multiple sclerosis. TAR DNA-binding protein 43 (TDP-43), which forms cytoplasmic aggregates that are a pathologic hallmark of amyotrophic lateral sclerosis, interacts with CD14 receptors and promotes the activation of nuclear factor κB (NF-κB) pathways. This leads to expression of NLRP3 mRNA, inflammasome activation, and production of caspase-1 and interleukins (e.g., IL-1β)

explored as potential targets, including enzymes, intracellular signaling molecules, and various receptors (i.e., G-protein coupled, ionotropic, and immunoglobulin receptors) [32]. For instance, the P2X ligand-gated ion channel type 7 (P2X7R), which is upregulated in innate immune cells and astrocytes, promotes inflammasome formation and is a promising target [33].

Amyloid/Tau Imaging

Alzheimer's disease (AD) is a neurodegenerative disease with pathologic hallmark deposition of extracellular neuritic plaques comprised of amyloid-β protein (Aβ) aggregates (Fig. 6.7) and intracellular neurofibrillary tangles (NFTs) comprised of hyperphosphorylated tau (Fig. 6.8) [4, 34–36]. Several PET radioligands have been developed in the last two decades for the noninvasive imaging of Aβ plaque burden in support of AD diagnosis in patients with dementia. The most studied and applied tracer for PET imaging of cerebral Aβ pathology is [^{11}C]Pittsburgh compound-B (PiB). The very short physical half-life (20 min) of ^{11}C requires an onsite cyclotron for isotope production, which thus prevents widespread clinical use. [^{11}C]PiB, a benzothiazole derivative, demonstrates selective high-affinity binding to insoluble fibrillary Aβ (but not to amorphous amyloid plaques and NFTs) in patients with AD. High cortical binding has been reported in >90% patients with a clinical diagnosis of AD [37]. This success led to the development of an ^{18}F-labeled analog with a longer half-life (110 min) and potential for more widespread clinical use that would behave similarly to [^{11}C]PiB. These efforts led to the development of [^{18}F]

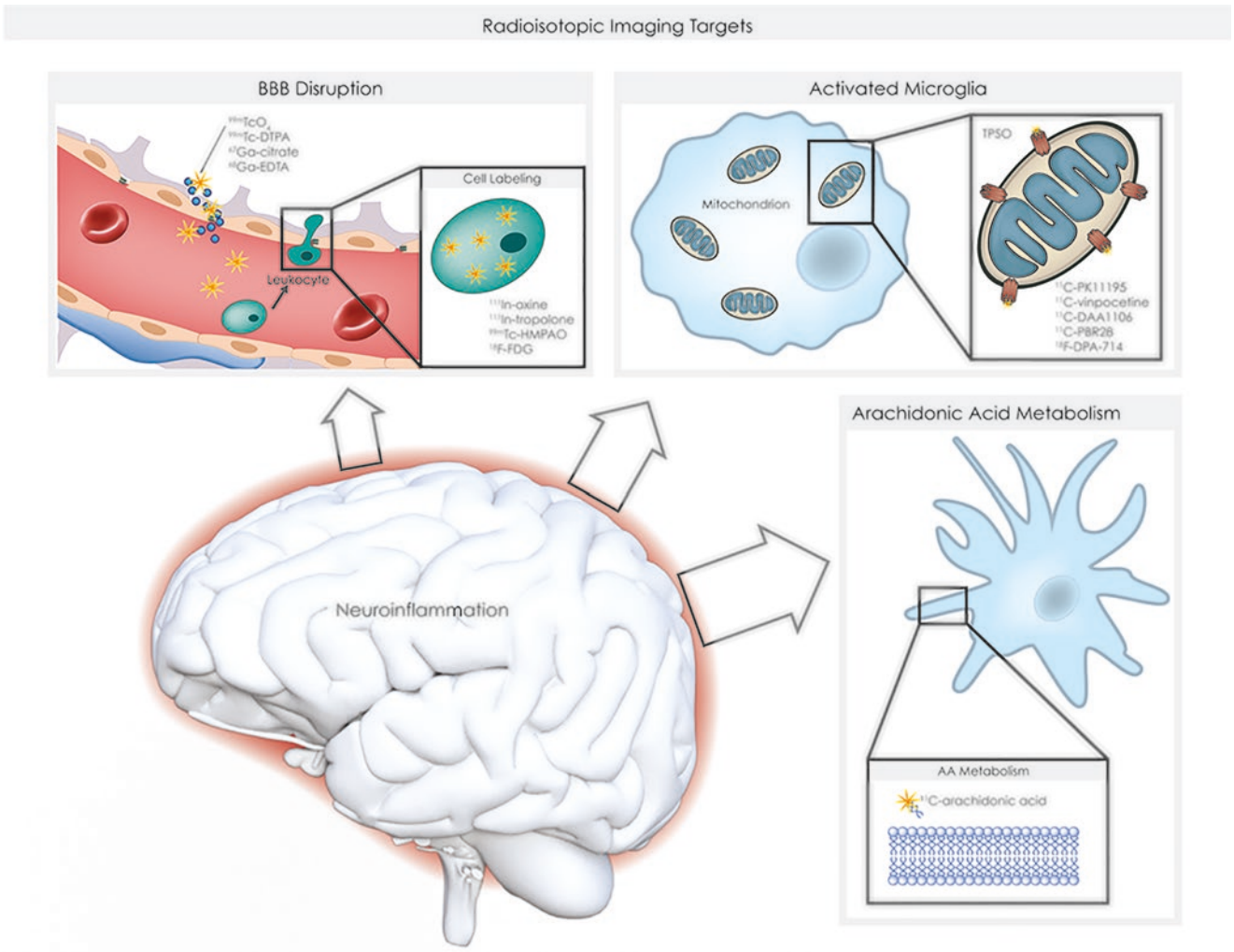

Fig. 6.6 Imaging for neuroinflammation. *Upper left:* Blood-brain barrier (BBB) disruption and permeable vessels allow leakage of radioisotopes. Radioisotope-labeled peripheral leukocytes are recruited and cross the BBB. *Top right:* Activated microglia upregulate mitochondrial translocator protein (TSPO). *Bottom right:* Arachidonic acid found in cell membranes is metabolized in the inflammatory process

Flutemetamol (trade name: Vizamyl), which is another benzothiazole derivative. Two other ^{18}F-labeled amyloid tracers are [^{18}F]Florbetapir (trade name: AMYViD) and [^{18}F]Florbetaben (trade name: Neuraceq), which are polyethylene glycol derivatives. All these ^{18}F-labeled tracers show high-affinity binding to fibrillar Aβ similar to PiB, however, with nearly twice the nonspecific white matter uptake. Most of the uptake is cleared via the liver and GI tract and with some contribution from renal excretion. In the spring of 2020, the FDA approved the first PET agent for tau imaging called [^{18}F]Flortaucipir (trade name: Tauvid). This agent aids in estimation of density and distribution of tau NFTs in patients with AD, with cortical retention consistent to known distributions of tau in AD, low white matter binding, and a strong association with AD severity [38]. Some limitations of this tracer include difficulty with reliable quantification and off-target binding outside the brain (including melanin and hemorrhage binding).

Conclusion

Advances in cellular/molecular biology, genetics, and imaging technology have expanded the clinical utility of molecular imaging. MI can illuminate the functional underpinnings of disease beyond structural changes and holds the promise of more timely and accurate disease diagnosis, personalized therapy optimization, and monitoring treatment response versus disease progression. Challenges in MI include agent stability, delivery efficiency, sensitivity, specificity (i.e., avoiding non-targeted uptake), and signal-to-noise ratio, to name a few. As MI emerges on the clinical scene of neuroimaging, a familiarity with MI agents, imaging techniques, mechanism and kinetics, and their limitations will help radiologists in study interpretation. The field is rapidly evolving and has stirred excitement in clinical and research arenas. Subsequent chapters will delve in greater detail with regard to this clinical and preclinical molecular neuroimaging. Buckle up!

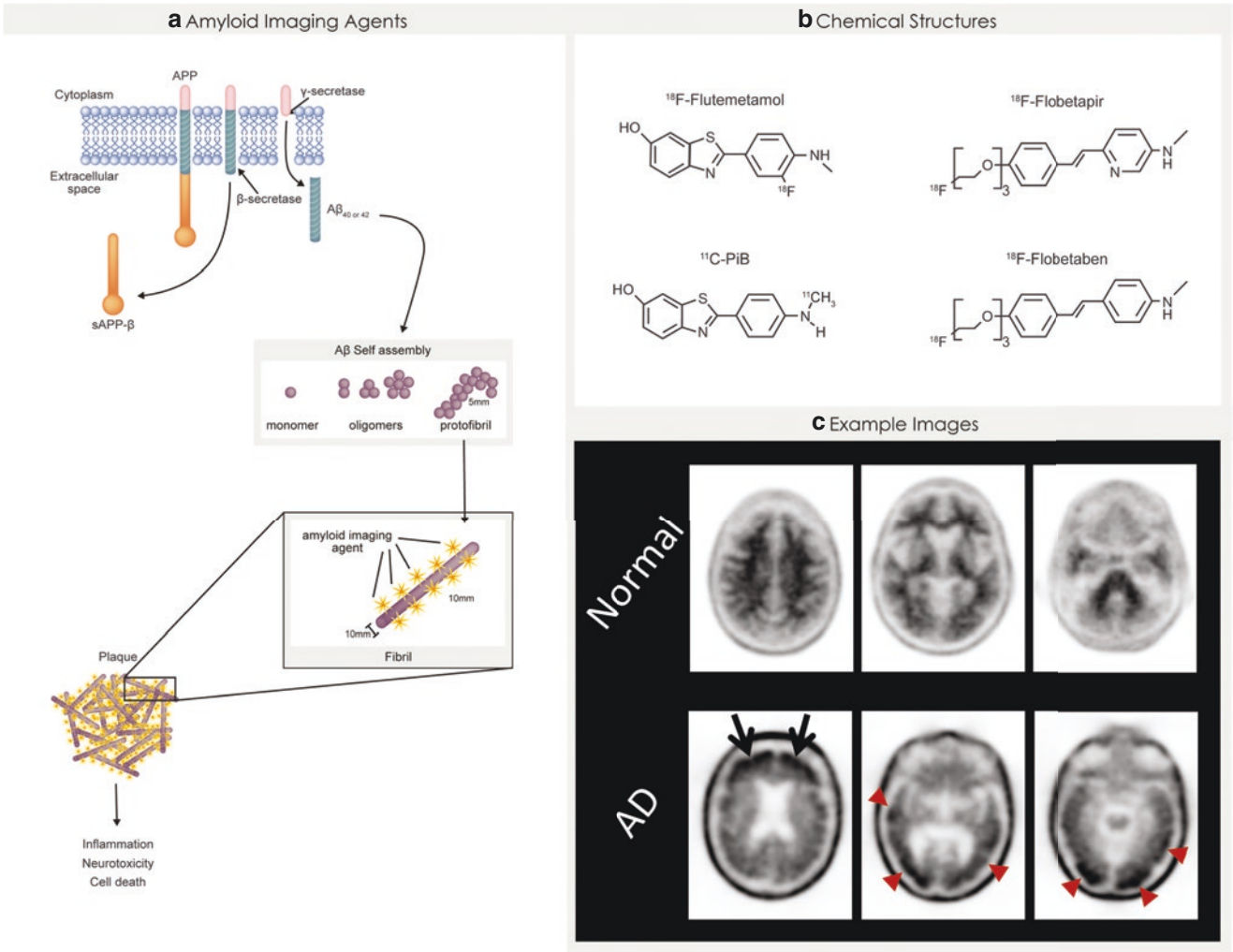

Fig. 6.7 MI targets in Alzheimer's disease (AD): amyloid imaging. (**a**) Amyloid precursor protein (APP) is cleaved by transmembrane proteases (β-secretase and γ-secretase) to form Aβ monomer (predominantly either Aβ40 or Aβ42). Aβ self-assembles into oligomers and protofibrils and the eventual formation of fibrils that comprise plaques. These fibrils exhibit a β-pleated sheet secondary structure. Amyloid imaging agents, such as [^{18}F]Florbetapir (Amyvid), are posited to interact with specific amino acid residues present in this β-sheet conformation and thus account for its signal accumulation in plaques. (**b**) Molecular structures of the most common research and clinically implemented amyloid imaging agents. (**c**) Axial [^{18}F]Florbetapir amyloid PET images from two different age-matched patients. Top row of images shows PET from a 73-year-old woman with a history of 2 years of cognitive decline. Normal [^{18}F]Florbetapir scan, with background white matter uptake. Bottom row PET images from a 75-year-old woman with a history of mild cognitive impairment and inability to tend to daily functional tasks. [^{18}F]Florbetapir scan shows diffusely increased radiopharmaceutical uptake throughout the cortical cerebral gray matter. The degree of abnormal uptake is most pronounced in frontal lobes (black arrows) in addition to the occipitotemporal regions (dark red arrowheads). The cerebellum has no evidence of abnormal uptake (not shown). These findings are consistent with moderate to frequent neuritic plaques, which can be seen in the setting of Alzheimer's disease (AD)

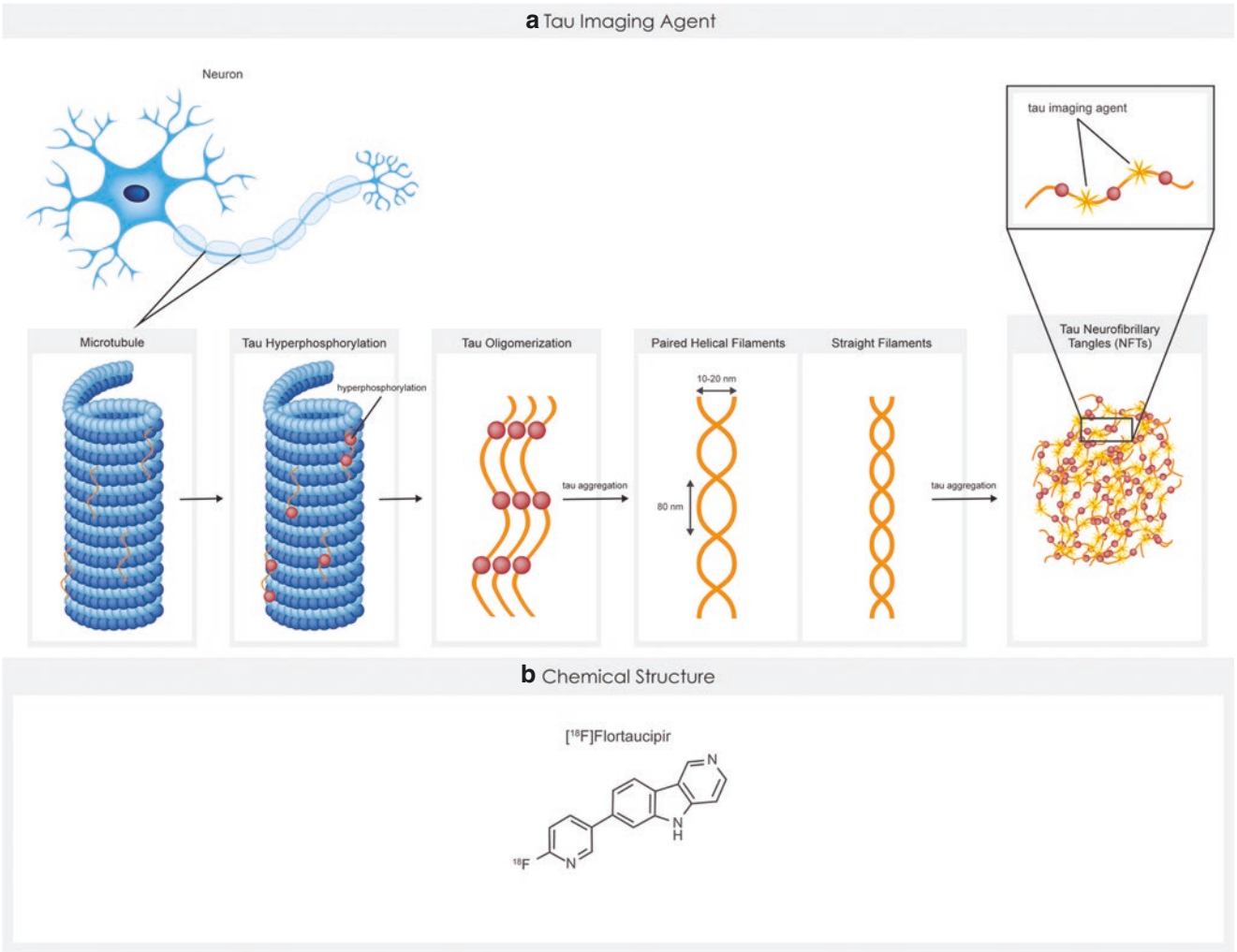

Fig. 6.8 MI targets in Alzheimer's disease (AD): tau Imaging. (**a**) In tauopathies, tau becomes hyperphosphorylated and detaches from microtubules. Phosphorylated tau then aggregates to form paired helical filaments (PHF) and straight filaments, with the eventual formation of neurofibrillary tangles (NFTs). These NFTs exhibit a β-pleated sheet secondary structure. Tau imaging agents, such as [^{18}F]Flortaucipir (Tauvid), are posited to bind to this β-sheet conformation and thus account for its signal accumulation in NFTs. (**b**) Molecular structure of the first FDA-approved tau imaging agent [^{18}F]Flortaucipir

Acknowledgments We thank Amy Thomas for her help designing many of the illustrations used in this book chapter.

References

1. Winnard P Jr, Raman V. Real time non-invasive imaging of receptor-ligand interactions in vivo. J Cell Biochem. 2003;90(3):454–63.
2. Malone C, Newton IG. Molecular imaging: the convergence of form and function. Appl Radiol. 2018;47:14–24.
3. Savariar EN, Felsen CN, Nashi N, Jiang T, Ellies LG, Steinbach P, et al. Real-time *in vivo* molecular detection of primary tumors and metastases with ratiometric activatable cell-penetrating peptides. Cancer Res. 2013;73(2):855–64.
4. Vallabhajosula S. Positron emission tomography radiopharmaceuticals for imaging brain Beta-amyloid. Semin Nucl Med. 2011;41(4):283–99.
5. Darcourt J, Schiazza A, Sapin N, Dufour M, Ouvrier MJ, Benisvy D, et al. 18F-FDOPA PET for the diagnosis of parkinsonian syndromes. Q J Nucl Med Mol Imaging. 2014;58(4):355–65.
6. Bell C, Dowson N, Puttick S, Gal Y, Thomas P, Fay M, et al. Increasing feasibility and utility of 18F-FDOPA PET for the management of glioma. Nucl Med Biol. 2015;42(10):788–95.
7. Stormezand GN, Glaudemans AWJM, Slart RHJA, Dierckx RAJO. Incidental meningioma detected with [18F]-FDOPA PET/CT. Eur J Hybrid Imaging. 2018;2(1):23.
8. Pagano G, Ferrara N, Brooks DJ, Pavese N. Age at onset and Parkinson disease phenotype. Neurology. 2016;86(15):1400–7.
9. Antonini A, Leenders KL, Vontobel P, Maguire RP, Missimer J, Psylla M, et al. Complementary PET studies of striatal neuronal function in the differential diagnosis between multiple system atrophy and Parkinson's disease. Brain J Neurol. 1997;120(Pt 12):2187–95.
10. Antonini A, Leenders KL, Eidelberg D. [11C]raclopride-PET studies of the Huntington's disease rate of progression: relevance of the trinucleotide repeat length. Ann Neurol. 1998;43(2):253–5.

11. Farde L, Wiesel FA, Halldin C, Sedvall G. Central D2-dopamine receptor occupancy in schizophrenic patients treated with antipsychotic drugs. Arch Gen Psychiatry. 1988;45(1):71–6.
12. Tateno A, Arakawa R, Okumura M, Fukuta H, Honjo K, Ishihara K, et al. Striatal and extrastriatal dopamine D2 receptor occupancy by a novel antipsychotic, blonanserin: a PET study with [11C]raclopride and [11C]FLB 457 in schizophrenia. J Clin Psychopharmacol. 2013;33(2):162–9.
13. Hagberg G, Gefvert O, Bergström M, Wieselgren IM, Lindström L, Wiesel FA, et al. N-[11C]methylspiperone PET, in contrast to [11C]raclopride, fails to detect D2 receptor occupancy by an atypical neuroleptic. Psychiatry Res. 1998;82(3):147–60.
14. Nordström AL, Farde L, Wiesel FA, Forslund K, Pauli S, Halldin C, et al. Central D2-dopamine receptor occupancy in relation to antipsychotic drug effects: a double-blind PET study of schizophrenic patients. Biol Psychiatry. 1993;33(4):227–35.
15. Nutt DJ, Lingford-Hughes A, Erritzoe D, Stokes PRA. The dopamine theory of addiction: 40 years of highs and lows. Nat Rev Neurosci. 2015;16(5):305–12.
16. Muhr C. Positron emission tomography in acromegaly and other pituitary adenoma patients. Neuroendocrinology. 2005;83(3–4):205–10.
17. Brown RK, Bohnen NI, Wong KK, Minoshima S, Frey KA. Brain PET in suspected dementia: patterns of altered FDG metabolism. Radiographics. 2014;34(3):684–701.
18. Kato T, Shinoda J, Nakayama N, Miwa K, Okumura A, Yano H, et al. Metabolic assessment of gliomas using 11C-methionine, [18F] fluorodeoxyglucose, and 11C-choline positron-emission tomography. Am J Neuroradiol. 2008;29(6):1176.
19. Hotta M, Minamimoto R, Miwa K. 11C-methionine-PET for differentiating recurrent brain tumor from radiation necrosis: radiomics approach with random forest classifier. Sci Rep. 2019;9(1):15666.
20. Floeth FW, Pauleit D, Sabel M, Stoffels G, Reifenberger G, Riemenschneider MJ, et al. Prognostic value of *O*-(2-[18F]-fluoroethyl)-L-tyrosine-positron emission tomography imaging for histopathologic characteristics and progression-free survival in patients with low-grade glioma. J Nucl Med. 2007;48(4):519–27.
21. Heijtel DFR, Mutsaerts HJMM, Bakker E, Schober P, Stevens MF, Petersen ET, et al. Accuracy and precision of pseudo-continuous arterial spin labeling perfusion during baseline and hypercapnia: a head-to-head comparison with 15O H2O positron emission tomography. Neuroimage. 2014;92:182–92.
22. Fan AP, Jahanian H, Holdsworth SJ, Zaharchuk G. Comparison of cerebral blood flow measurement with [15O]-water positron emission tomography and arterial spin labeling magnetic resonance imaging: a systematic review. J Cereb Blood Flow Metab. 2016;36(5):842–61.
23. Gupta A, Chazen JL, Hartman M, Delgado D, Anumula N, Shao H, et al. Cerebrovascular reserve and stroke risk in patients with carotid stenosis or occlusion: a systematic review and meta-analysis. Stroke. 2012;43(11):2884–91.
24. Wyss-Coray T, Mucke L. Inflammation in neurodegenerative disease--a double-edged sword. Neuron. 2002;35(3):419–32.
25. Frank-Cannon TC, Alto LT, McAlpine FE, Tansey MG. Does neuroinflammation fan the flame in neurodegenerative diseases? Mol Neurodegener. 2009;4:47.
26. Jain P, Chaney AM, Carlson ML, Jackson IM, Rao A, James ML. Neuroinflammation PET imaging: current opinion and future directions. J Nucl Med. 2020;61(8):1107–12.
27. Voet S, Srinivasan S, Lamkanfi M, van Loo G. Inflammasomes in neuroinflammatory and neurodegenerative diseases. EMBO Mol Med. 2019;11(6):e10248.
28. Esposito G, Giovacchini G, Liow J-S, Bhattacharjee AK, Greenstein D, Schapiro M, et al. Imaging neuroinflammation in Alzheimer's disease with radiolabeled arachidonic acid and PET. J Nucl Med. 2008;49(9):1414–21.
29. Cagnin A, Brooks DJ, Kennedy AM, Gunn RN, Myers R, Turkheimer FE, et al. In-vivo measurement of activated microglia in dementia. Lancet (London, England). 2001;358(9280):461–7.
30. Turner MR, Cagnin A, Turkheimer FE, Miller CC, Shaw CE, Brooks DJ, et al. Evidence of widespread cerebral microglial activation in amyotrophic lateral sclerosis: an [11C](R)-PK11195 positron emission tomography study. Neurobiol Dis. 2004;15(3):601–9.
31. Gerhard A, Banati RB, Goerres GB, Cagnin A, Myers R, Gunn RN, et al. [11C](R)-PK11195 PET imaging of microglial activation in multiple system atrophy. Neurology. 2003;61(5):686–9.
32. Narayanaswami V, Dahl K, Bernard-Gauthier V, Josephson L, Cumming P, Vasdev N. Emerging PET radiotracers and targets for imaging of neuroinflammation in neurodegenerative diseases: outlook beyond TSPO. Mol Imaging. 2018;17:1536012118792317.
33. Han J, Liu H, Liu C, Jin H, Perlmutter JS, Egan TM, et al. Pharmacologic characterizations of a P2X7 receptor-specific radioligand, [11C]GSK1482160 for neuroinflammatory response. Nucl Med Commun. 2017;38(5):372–82.
34. Herholz K, Ebmeier K. Clinical amyloid imaging in Alzheimer's disease. Lancet Neurol. 2011;10(7):667–70.
35. Vlassenko AG, Benzinger TL, Morris JC. PET amyloid-beta imaging in preclinical Alzheimer's disease. Biochim Biophys Acta. 2012;1822(3):370–9.
36. Mason NS, Mathis CA, Klunk WE. Positron emission tomography radioligands for *in vivo* imaging of Aβ plaques. J Label Compd Radiopharm. 2013;56(3–4):89–95.
37. Rabinovici GD, Jagust WJ. Amyloid imaging in aging and dementia: testing the amyloid hypothesis *in vivo*. Behav Neurol. 2009;21(1):117–28.
38. Lois C, Gonzalez I, Johnson KA, Price JC. PET imaging of tau protein targets: a methodology perspective. Brain Imaging Behav. 2019;13(2):333–44.
39. Filss CP, et al. Amino acid PET and MR perfusion imaging in brain tumours. Clin Transl Imaging. 2017;5(3):209–23.
40. Ishii Y, et al. Simultaneous phase-contrast MRI and PET for non-invasive quantification of cerebral blood flow and reactivity in healthy subjects and patients with cerebrovascular disease. J Magn Reson Imaging. 2020;51(1):183–94.